JOURNAL OF GEOPHYSICAL RESEARCH, VOL. 102, NO. C12, PAGES 26,383–26,396, NOVEMBER 30, 1997

Temperature, accumulation, and ice sheet elevation in central Greenland through the last deglacial transition

Kurt M. Cuffey

Department of Geological Sciences, University of Washington, Seattle

Gary D. Clow

Climate History Program, U.S. Geological Survey, Denver, Colorado

Abstract. We present a combined heat- and ice-flow model, constrained by measurements of temperature in the Greenland Ice Sheet Project 2 (GISP2) borehole and by the GISP2 $\delta^{18}O$ record and depth-age scale, which determines a history of temperature, accumulation rate, and ice sheet elevation for the past 50,000 years in central Greenland. Important results are: that the temperature increase from average glacial to Holocene conditions was large, approximately 15 °C, with a 20 °C warming from late glacial to Holocene; that the average accumulation rate during the last glacial maximum (between 15 and 30 kyr B. P.) was 5.5 to 7 cm yr^{-1}, approximately 25% of the modern accumulation rate; that long-term (500-1000 years) averaged accumulation rate and temperature have been inversely correlated during the most recent 7 millennia of the Holocene; and that the Greenland Ice Sheet probably thickened during the deglacial transition. The inverse correlation of accumulation rate and temperature in the mid and late Holocene suggests that the Greenland Ice Sheet is more prone to volume reduction in a warmed climate than previously thought and demonstrates that accumulation rate is not a reliable proxy for temperature. The elevation history of the ice sheet is poorly constrained by the model, and independent evidence is needed. We also present a simple estimate of the response time for thinning of the interior region of an ice sheet due to retreat of its margins. This was approximately 1900 years for central Greenland during deglaciation.

Introduction

Inferences of past temperatures, accumulation rates, and ice sheet elevations from ice-core paleoclimate studies are inextricably linked. Temperature at depth in the ice sheet, analysis of which provides the most direct measure of ancient temperatures, depends profoundly on the vertical advection of heat by ice flow, which in turn depends on accumulation rates via ice sheet geometry. Accumulation rates inferred by destraining observed layer thicknesses depend on the history of ice sheet thickness and deformation, which depend both on temperature and accumulation rate. Ice sheet elevations are determined by temperature and accumulation rate and their patterns, through the filter of ice dynamics, and also depend on the isostatic response of the lithosphere and on sea level changes.

A linked approach to inferring these important parameters is therefore necessary, and this paper presents a coupled heat- and ice-flow model, applicable to the flow divide regions of ice sheets, for this purpose. We present results constrained by measurements from the Greenland Ice Sheet Project 2 (GISP2) core and borehole: the temperature-depth profile of G.D. Clow [*Clow et al.*, 1996], the $\delta^{18}O$ ratios of P.M. Grootes and M. Stuiver [*Grootes et al.*, 1993], and the depth-age scale of *Alley et al.* [1993], *Meese et al.* [1994], and *Bender et al.* [1994]. The model output is an approximate temperature history, which is a calibrated version of the oxygen isotope record, and a field of possible accumulation rate and elevation histories. The accumulation and elevation cannot be determined precisely due to uncertainties in important ice dynamical parameters. Measurements of total gas content may provide an independent elevation history [*Raynaud and Lebel*, 1979], which will then allow the accumulation history to be better constrained.

Our analysis has revealed that the warming from average glacial to the Holocene was large, approximately 15°C [*Cuffey et al.*, 1995] a value twice that inferred from isotopic thermometry. An independent study using Greenland Ice Core Project data [*Johnsen et al, 1995*] confirms this result. An important ques-

Copyright 1997 by the American Geophysical Union.

Paper number 96JC03981.
0148-0227/97/96JC-03981$09.00

tion remains concerning how well this change of ice sheet surface temperature represents the change in atmospheric temperature through the troposphere above the ice sheet, given that the strength of near-surface temperature inversions may also have changed considerably. Below, we briefly address this question of inversion strength, but do not resolve it.

In this paper we complete the presentation, begun in *Cuffey et al.* [1995], of the temperature history, and in addition focus on the history of ice sheet thickness and elevation, the accumulation rate during the last glacial maximum, and the relationship between accumulation rate and temperature during the Holocene. We begin by fully presenting the model and the $\delta^{18}O$ calibration method. The model has five components: heat transfer and generation, surface temperature forcing, ice flow, thickness and elevation, and accumulation rates.

Here we present results for only the most recent 50 millennia of climate history. Results become increasingly speculative further back in time, due to masking of the surface temperature signal by the geothermal flux and by the choice of initial condition, and due to uncertainties in the thickness history resulting from poor knowledge of rheologic layering and deformation patterns deep in the ice sheet and from poor knowledge of ice sheet marginal position. The latter in particular is poorly known prior to the last glacial maximum, and we therefore present only 30 millennia of the thickness and elevation histories. The corresponding increase in uncertainty on the inferred accumulation and temperature histories is less pronounced because they depend on the integrated history of ice dynamics from then to present.

In this paper, we treat our calibrated isotopic history as synonymous with temperature, an assumption that is supported at a variety of temporal scales by a variety of methods [*Shuman et al,* 1995; *Cuffey et al,* 1995, 1994; *Jouzel et al.,* this issue]. High-resolution temperature histories that do not employ this assumption are being obtained by inversion of high-precision borehole temperature data (G.D. Clow, manuscript in preparation, 1996) and by a Monte Carlo inverse technique (D. Dahl-Jensen, manuscript in preparation, 1996) and will provide an important check on some of the results of this paper, as well as providing a wealth of new information about temperature changes through the last glacial maximum.

Model Components

Heat Transfer and Generation

We use a control volume mesh [*Patankar,* 1980] to solve the one-dimensional energy equation through 100,000 years of history:

$$\rho c(T)\frac{\partial T(z,t)}{\partial t} = \frac{\partial}{\partial z}\left[k(\rho,T)\frac{\partial T(z,t)}{\partial z}\right] - \rho c(T) w(z,T)\frac{\partial T(z,t)}{\partial z} + \tau \cdot \dot{\epsilon}(z,t) \qquad (1a)$$

$$T(z = H(t);t) = \frac{\delta^{18}O(t) - \beta}{\alpha}; \quad 100\text{kyr B.P.} < t < 0 \qquad (1b)$$

$$\frac{\partial T}{\partial z}(z = -10\text{ km}) = \frac{-q_g}{k_r} \qquad (1c)$$

$$T(z;t = 100\text{kyr B.P.}) = T_i[z; q_g, \bar{T}_p, H(t = 100\text{kyr B.P.}), \Delta T_p] \qquad (1d)$$

All variables are defined in the Notation list at the end of the text. The heat capacity and thermal conductivity depend on temperature and density according to *Yen* [1981]. The control volume method entails dividing the domain of interest into discrete blocks (each a "control volume"), and performing all calculations using quantities integrated within the blocks, and fluxes between the blocks. In our model, the topmost control volume stretches to accommodate thickness changes of the ice sheet. When it has stretched by 5 m, we create a new control volume above, which is initially assigned a negligible thickness. This new volume grows if the ice sheet subsequently thickens, or is destroyed if the ice sheet subsequently thins. The control volumes near the ice sheet surface which are created, stretched, and/or destroyed through time never exceed 10 m in depth. The mesh is finest near the surface of the ice sheet, to resolve the variable density, and near the bed, for accurate ice dynamics calculations. On average, there are approximately 130 control volumes within the ice sheet. Fifteen volumes extend downward into bedrock, to a depth of 10 km. Our time step is 40 years initially (100 to 15 kyr B.P.), and decreases to 2 years at 15 kyr B.P.

We generate the initial temperature profile, T_i, by first calculating a steady state profile, which we subject to several glacial-interglacial cycles (80 kyr of linearly decreasing temperature; 20 kyr of constant temperature interglacial) of amplitude ΔT_p and average temperature $\bar{T}_p$. We end this calculation with an interglacial followed by cooling of magnitude $1/2\Delta T_p$ and duration 5 kyr, representing the end of the Eemian. To limit computation time, we assume the thickness does not change, and that the vertical velocity at the surface changes in synchroneity with the temperature history, with a minimum glacial value of one third the Holocene value of 0.24 m yr^{-1}. By this method, we calculate T_i for several values of q_g, $\bar{T}_p$, ΔT_p, and H. Our temperature results back to 40 kyr B.P. are insensitive to values for all of these parameters; the first 60 kyr of isotope-derived forcing is sufficient to mask the initial condition, except deep in the borehole where the unknown geothermal flux dominates the temperature profile, obscuring paleoclimate information.

Our use of a one-dimensional heat flow model for these calculations is justified because horizontal temperature gradients in the ice are very small. The horizontal temperature gradient at the surface is extremely small, because the surface is nearly flat. The at-depth

temperature gradient due to horizontal gradients in vertical velocity is also very small, at locations greater than several ice thicknesses from the ice divide [*Paterson and Waddington*, 1986]. We do not know how the ice divide position has changed through time, though it has probably not been fixed [*Anandakrishnan et al.*, 1994]. It is also apparent from analysis of radar data that the strain rate pattern predicted by *Raymond* [1983] that would give rise to an at-depth temperature gradient either does not exist at the Greenland summit or exists but is obscured by migrations of the ice divide (E.D. Waddington et al., manuscript in preparation, 1996). The additional complexity of a two-dimensional model therefore is not warranted.

Surface Temperature Forcing

The surface temperature history is a combination of linear functions of the $\delta^{18}O$ record, calibrated against the measured temperature-depth profile using an inverse technique. We use 2-m-averaged isotope values. To choose which linear function(s) of the $\delta^{18}O$ record to use as the forcing, we compare modeled $T(z)$ with the borehole temperature measurements $\Theta(z)$ in the fluid-filled portion of the 3054m-deep hole by defining the mismatch index

$$J = \int_0^{2975} \frac{[T(z) - \Theta(z)]^2}{\sigma_t^2(z) + f\sigma_D^2(z)} dz \tag{2a}$$

$$\sigma_t^2(z) = \left[\int_0^{\infty} t^2 N_T(z,t) dt - \langle N_T \rangle \right]^{-1} \tag{2b}$$

$$\sigma_D^2(z) = \int_T U(\Delta T_\mu) * U(\Delta T_b) * U(\Delta T_i) T^2 dT - \langle U(\Delta T_\mu) * U(\Delta T_b) * U(\Delta T_i) \rangle \tag{2c}$$

and finding α, β, and q_g values for which J is minimized. The minimization is by a Levenberg-Marquardt technique. We allow some time variation of α and β by dividing the history into four periods, within which these parameters are held constant so that $\delta^{18}O$ is a linear function of T (equations (16a) to (16d)). All β values except one are determined by the requirement that temperature be continuous across the boundaries of these periods. Thus the minimization finds four values for α and one each for β and q_g.

The denominator of (2a) is a weighting function, with a trade-off parameter that allows either the upper part or lower part of the temperature profile to be weighted more heavily in the minimization, as explained henceforth. Here σ_D measures the sensitivity of the calculated temperature profile to poorly known model inputs, such as the ice fabric enhancement term ($\mu(z)$), ancient accumulation rates, and the variables that determine the initial temperature profile. We calculate modern temperature-depth profiles for maximum and minimum plausible values of the uncertain model parameters (for example, we set the softness enhancement for ice-age ice to $\mu = 1$ and to $\mu = 5$). The calculated temperature profiles then delimit, at any depth, a plausible range of values. We suppose that all temperatures within this range are equally valid, so the temperature deviation from our standard calculation (for which $\mu = 3$) is a uniform random variable, $U(\Delta T_\mu)$. A similar temperature deviation is associated with all the other uncertain variables, so we calculate the probability density function of the sum of all these uniform random variables representing temperature deviations about a standard model. If this summed density function is narrow, the weighting requires the model calculations to match the measurements closely. If this summed density function is wide, the temperature there is highly dependent on poorly known quantities, and a close match is not forced. As a measure of width, we use the variance of the density function. These widths increase with depth in the borehole.

However, deeper in the borehole, the temperature depends on a longer interval of the surface temperature history. This suggests the deep part of the borehole should receive more weight, and for this purpose we define σ_t. Here σ_t measures the inverse of the duration of surface temperature history that contributes to the temperature at depth z. $N_T(z,t)$ is the temperature response at z to a unit surface temperature pulse at $t = 0$. Using the inverse of its width (again defined by the variance) gives the desired weight.

We do not know how to best choose between these opposing weighting schemes, so we perform the minimization for a range of f values. For $f = 0$, the weighting function is a maximum at the bottom of the borehole, where it is 25 times the value at the top of the borehole. For $f = 100$, the weighting is maximum at approximately 2400 meters above the base of the ice sheet, and is 20 times the value at the bottom of the borehole. Fortunately, results depend only weakly on choice of f for a wide range of values $0 < f < 1000$ and therefore are not sensitive to how we pose the inverse problem (equation 2a) [*Cuffey et al.*, 1995]. This low sensitivity is evidence that the $\delta^{18}O$ record provides an appropriate template for the surface temperature forcing at a variety of time scales. The dependence of our results on uncertainties in physical variables is also low, and is presented in *Cuffey et al* [1995]. Note that these claims of low sensitivity are inseparable from our definition of the inverse problem; the preceding discussion of the weighting scheme is therefore important, if somewhat arcane.

Ice Flow

In our one-dimensional model, the important ice flow component that we must calculate is the vertical ice motion, which advects heat and determines, together with the snowfall rate, the thickness history of the ice sheet and the strain history of annual layers. Our vertical velocity is the product of a term that describes mass continuity for an ice sheet in steady state geometry (w_S), a nondimensional term w_M that accounts for the enhancement of vertical velocity due to the non-

steady response to distant changes in marginal position, and a nondimensional adjustment function w_A, which is a polynomial tuned so that our model depth-age scale matches that observed in the core:

$$w(z,t) \equiv w_S(z,t) w_M(t) w_A(z) \tag{3}$$

Writing the vertically integrated mass continuity equation, for an ice sheet with a density structure that is time invariant as a function of depth below the surface (i.e., the density profile moves up and down with the ice sheet surface, without changing shape), gives

$$-w_S(z,t) = \frac{1}{\rho(z,t)} \int_0^z \rho(z,t) \nabla_H \cdot \vec{u}(z,t) dz + \frac{1}{w_M w_A} \frac{\partial H}{\partial t} \left[\frac{\rho_i - \rho(z,t)}{\rho(z,t)} \right] \tag{4}$$

assuming that horizontal gradients in density are negligible. Thus the downward ice velocity at elevation z balances the horizontal mass-flux divergence below z (the first term on the right), with a small correction to allow mass redistribution as the density structure moves vertically, following changes in ice sheet thickness (the second term on the right). For $\rho(z)$ we use the measured density-depth profile from the GISP2 core [*Alley and Koci*, 1990].

On the basis of the Summit region topography and on measurements (K. Keller, unpublished data, University of Copenhagen, 1995), the horizontal flow is dominantly in a westerly direction (x), with some spreading to north and to south (y). We follow *Whillans and Cassidy* [1983] and *Bolzan et al.* [1995] in describing the spreading velocity as inversely proportional to the radius of curvature of topographic contours and directly proportional to the principal velocity

$$u_y = \frac{y}{R_T} u_x \tag{5}$$

$$\nabla_H \cdot \vec{u} = \frac{\partial u_x}{\partial x} + \frac{\partial u_y}{\partial y} = \frac{\partial u_x}{\partial x} + \frac{u_x}{R_T} \tag{6}$$

The westward velocity is the integral from the bed upward of shear strain rate. Assuming Glen's flow law with $n = 3$ this is

$$u_x(z,t) = 2A_o \times \int_0^z \mu(z,t) \exp\left[\frac{-Q}{RT(z,t)} \right] (\tau_{xz}^2 + \tau_a^2) \tau_{xz} \, dz \tag{7}$$

and its gradient is

$$\frac{\partial u_x}{\partial x} = 2A_o \times \left[3 \int_0^z \mu(z,t) \exp\left(\frac{-Q}{RT(z,t)} \right) \tau_{xz}^2 \frac{\partial \tau_{xz}}{\partial x} \, dz + \int_0^z \mu(z,t) \exp\left(\frac{-Q}{RT(z,t)} \right) \times \left(\tau_a^2 \frac{\partial \tau_{xz}}{\partial x} + 2\tau_a \tau_{xz} \frac{\partial \tau_a}{\partial x} \right) dz \right] \tag{8}$$

The accessory stresses τ_a are very small compared to τ_{xz} in the lower half of the ice sheet where most of the deformation occurs, so their contribution to the integral quantities is negligible and they may be neglected at GISP2. We use them in the heat generation term of (1) for calculating the steady state profile but do not use them otherwise. Neglecting τ_a in the 100-kyr model runs affects the final calculated temperature profile by about 1 mK and affects the thickness history by no more than a few meters. (For calculations that included τ_a, we assumed an initial vertical velocity profile and, at each time step, iteratively solved for stresses and deformations until convergence was attained.)

The ice-softness enhancement, $\mu(z,t)$, is a poorly known term that accounts for the softening effect of vertically oriented crystal fabrics and possibly chemical impurities on horizontal simple shear flow [*Paterson*, 1991]. We allow two kinds of ice: ice-age ice, which attains a maximum value of 3, and interglacial ice, which attains a maximum value of 1.5. For both, μ increases linearly from a value of 1 at the surface to its maximum value midway through the ice sheet, and maintains this value at all greater depths. We arbitrarily assume that ice-age ice deposits when 5-kyr-averaged $\delta^{18}O < -38$. The depths of the boundaries between ice-age and interglacial ices are recalculated at each time step.

We assume that gradients in longitudinal deviatoric stresses are not important, and assume the vertical normal stress balances the weight of overburden. The shear stress and its gradient are thus given by the standard formulae

$$\tau_{xz} = -g\bar{\rho} \frac{\partial H}{\partial x} (H - z) \tag{9a}$$

$$\frac{\partial \tau_{xz}}{\partial x} = -g\bar{\rho}(H - z) \frac{\partial^2 H}{\partial x^2} - g\bar{\rho} \left(\frac{\partial H}{\partial x} \right)^2 \tag{9b}$$

In calculating w_S, we assume the ice sheet maintains a steady state profile according to the model of *Vialov* [1958]. Differentiating the Vialov thickness profile gives expressions for $\partial H/\partial x$ and $\partial^2 H/\partial x^2$ in terms of H and L (the distance across the ice sheet from margin to divide), and we use these in (9a) and (9b). Initial values for H and $\partial H/\partial x$ are determined iteratively so that the final values match the modern observed ones (a steepest-descent inverse technique rescues us from the inherent clumsiness of such a procedure). The initial $\partial^2 H/\partial x^2$ is chosen so the ice sheet is initially in steady state with the accumulation rate.

This description of local geometric changes is incomplete. As the ice sheet margins change position, evolution from one steady ice sheet configuration to another requires transient changes in ice flux which are not permitted by steady state geometries. In our calculations, the ice sheet margins retract during deglaciation, as indicated by geologic evidence [*Funder*, 1989; *Funder and Larsen*, 1989]. We use a linear retreat from $L_o + \Delta L$ km at 14 kyr B.P. to $L_o = 400$ km at 7 kyr B.P., where ΔL ranges from 0 to 200 km. This causes a wave of thinning to propagate inland (e.g., *Alley and Whillans*, 1984). A

transient increase in ice flux divergence must accompany this thinning. We approximate the ice sheet as a purely linear and diffusive system (the diffusive term dominates in the Alley and Whillans model for deep ice with a low surface slope). The ice sheet elevation change through time due to a small marginal retreat is then analogous to the temperature change in a solid slab bounded by two parallel planes following a small negative step change in boundary temperature on one side, given an insulated boundary on the other side. The insulated side corresponds to the summit region of the ice sheet. Using this analogy, we define the thickness response $\Lambda(t-t^*)$ at GISP2 through time t to a unit marginal retreat at time t^* as (compare equation (5) of *Carslaw and Jaeger* [1959, p. 101])

$$\Lambda(t-t^*) \equiv 2\sum_{j=0}^{\infty} \frac{(-1)^j}{\omega_j L} \exp\left[-\gamma\omega_j^2(t-t^*)\right] \; ; \qquad \omega_j = \frac{(2j+1)\pi}{2L} \tag{10a}$$

This thinning is due to an enhancement of the ice flux divergence, which for the standard one-dimensional Glen's law laminar flow ice sheet is [*Paterson*, 1994, p. 252 and 256]

$$\frac{\partial H}{\partial t} = \mathcal{S}\frac{\partial H}{\partial x} + \hat{\gamma}\frac{\partial^2 H}{\partial x^2}; \qquad \hat{\gamma} = \frac{2n}{n+2}\bar{A}(\rho_i g)^n H^{n+2}\left(\frac{\partial H}{\partial x}\right)^{n-1} \tag{10b}$$

$\mathcal{S}$ is a wave speed, and $\hat{\gamma}$ is the local diffusivity. To approximate the diffusivity γ in (10a), we average $\hat{\gamma}$ across the ice sheet from margin to summit and eliminate $\partial H/\partial x$ by assuming a constant basal yield stress of $\rho g H(\partial H/\partial x) = \tau_0 = 1$ bar.

$$\gamma \approx \frac{1}{L}\int_L \hat{\gamma}(x)\, dx \approx \frac{6}{5}\bar{A}\rho_i g(0.8H_d)^3\tau_0{}^2 \approx 1.86 \text{ m}^2\text{s}^{-1} \tag{10c}$$

For $\bar{A}$ we use a typical value for -10 °C [*Paterson*, 1994] multiplied by an enhancement factor of 2.5 for ice-age ice ($\bar{A} = 1.25 \times 10^{-24}$; $H_d = 3000$ m).

According to this formulation, the thinning of the ice divide following an abrupt retraction of the margins is at first slow, then rapid as the thinning wave reaches the divide, and then slow again as the thickness approaches the new steady value (Figure 1). After a time τ_M, the divide has thinned to within $1/e$ of its final value. Here τ_M is easily discerned by recognizing the $j = 0$ term in the sum in (10a) as dominant late in the response, and is

$$\tau_M \approx \left(1 + \ln\frac{4}{\pi}\right)\frac{4L^2}{\gamma\pi^2} \approx \frac{0.82L^2}{\bar{A}\rho_i g H_d^3 \tau_0^2} \tag{10d}$$

which was approximately 1900 years for Summit during the deglacial retreat ($L = 470$ km). Despite the gross

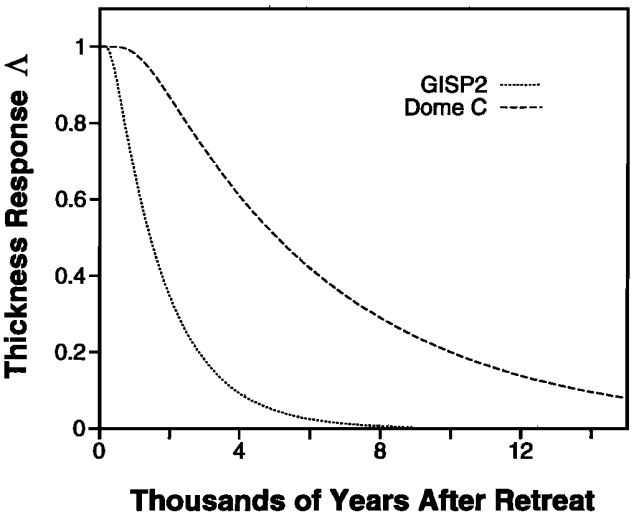

Figure 1. The filter $\Lambda(t-t^*)$ describing the change in ice divide thickness due to a step unit retreat of the ice sheet margin at time t^*, for GISP2 and Dome C, Antarctica.

approximations required to obtain this formula (particularly ignoring the wave component in (10c)) both the form of the response and the predicted timescale compare favorably with results from the fully two-dimensional ice sheet model of *Alley and Whillans* [1984] for Dome C, Antarctica (Figure 1; compare to their Figures 1 and 4, curve d). Using the values quoted by them for $\bar{A} = 8 \times 10^{-25}$, $L = 930$km, and $H_d = 3600$ m, our approximation (10d) indicates a response time of $\tau_M \approx 6700$ years for Dome C, compared to 8000 years from *Alley and Whillans* [1984, p. 6492]. Unfortunately, τ_M is sensitive to the effective ice sheet softness, $\bar{A}$, which is a poorly known quantity for real ice sheets. One could obtain an alternative, possibly more reliable estimate of the diffusivity that does not contain $\bar{A}$ by using ice fluxes (Φ) derived from integrated accumulation rates and $\hat{\gamma} = n\Phi(\partial H/\partial x)^{-1}$.

To calculate the rate of thickness change ($\dot{H}_M$) at Summit resulting from an arbitrary history of marginal retreat dL/dt, we integrate the unit responses through time, accounting for the dependence of steady state thickness on the square root of L in the Vialov model

$$\dot{H}_M = \frac{d}{dt}\left[\frac{H(t_r)}{2\sqrt{L(t_r)}} \times \int_{t_r}^{t} \frac{1}{\sqrt{L(t^*)}}\frac{dL(t^*)}{dt^*}\Lambda(t-t^*)\, dt^*\right] \tag{10e}$$

The corresponding increase of the vertical velocity at the surface of the ice sheet is $\dot{H}_M\rho_i/\rho(H)$ and the nondimensional vertical velocity enhancement in (3) is

$$w_M(t) \equiv \left[1 + \frac{\dot{H}_M\rho_i}{w_s(H)\rho(H)}\right] \tag{11}$$

We neglect the small contribution of this transient motion to the heat generation term in (1a).

Although we have attempted to calculate the vertical velocity in a physically meaningful fashion, there are many uncertainties in this calculation. Ice rheology is poorly known, particularly because enhancement of strain rate due to impurity content and crystal fabric is not well known. Ice close to the bed under GISP2 originated close to the ice divide, where the vertical strain rate differs from the flank flow setting calculated here. The ice divide has probably moved through time, following an unknown path. The accumulation rate prior to 50 kyr B.P. is poorly known. Changes in the horizontal flux divergence induced by changes in accumulation gradients, or rheologic gradients, are not known.

We attempt to isolate the temperature calculation from the effects of this uncertainty in a simple fashion by introducing an adjustment function that we tune so the depth-age relation observed in the core is matched by our model prediction, for any given accumulation history and choices of ice dynamical parameters. We find that a quadratic function of depth provides sufficient tuning power to match the depth age scale to within 10 m in our sensitivity tests [*Cuffey et al.*, 1995]. We test the match at eight depths, the deepest of which is 2800 m. The function is

$$w_A(z) = a_1 \left(\frac{z}{H}\right)^2 + a_2 \left(\frac{z}{H}\right) + a_3; \;\; w_A(H) = 1.0 \quad (12)$$

and the a are adjustable.

Thickness and Elevation Changes

The ice sheet at GISP2 will thicken if the depth of snow added to the ice sheet surface per time (by snowfall and advection) exceeds the downward vertical velocity at the surface. Thus the thickness changes at a rate

$$\frac{\partial H}{\partial t} = \dot{b}(t) - \frac{\rho(H)}{\rho_i}\frac{\partial H}{\partial x}u_x(H) - \frac{1}{\rho_i}\int_0^H \rho(z)\nabla_H \cdot \vec{u}(z)\, dz - \dot{H}_M \quad (13)$$

Here the first and second terms on the right are the ice accumulation rate and thickness advection from upstream, respectively. The third term is the vertical velocity for steady geometry, and the fourth term is the transient velocity response to distant changes in marginal position.

To convert the thickness history to an elevation history, we add an approximate history of sea level changes with a maximum sea level depression of 120 m [*Shackleton*, 1987; *Fairbanks*, 1989]. Following *Johnsen et al.* [1995], we also parameterize the isostatic response of the Greenland crust to changes in vertical load as an exponential decay with a time constant of 5000 years [*Cathles*, 1975]. Using a single response time is not strictly correct [*Peltier and Hyde*, 1987], but the isostatic adjustment is small compared to the uncertainties introduced by the poorly known ice dynamical parameters. We also do not consider horizontal spatial gradients in the isostatic response, which will act to lower the surface slope of the ice sheet.

Accumulation Rate History

For times more recent than 50 kyr B.P., we calculate the accumulation rate by dividing observed layer thickness λ_t by an estimate of strain. The vertical normal strain rate, $\dot{\epsilon}_{zz}$, which causes the thinning of layers, is proportional to its depth average

$$\dot{\epsilon}_{zz}(z,t) \equiv \Upsilon(z,t)\frac{w(H,t)}{H(t)} \quad (14)$$

Most of the deformation in the ice sheet occurs in its lower third (G.D. Clow and N. Gundestrup, unpublished manuscript, 1996). The proportionality function $\Upsilon(z,t)$, which describes the shape of the strain rate versus depth curve, is therefore nearly constant in the upper two thirds, and consequently, in this region, most of the time variation of $\dot{\epsilon}_{zz}$ is due to variation in $w(H,t)$ and $H(t)$. Therefore we approximate

$$\dot{b}(t) = \lambda_t \exp\left\{\int_t^{t_p} \Upsilon[z_t(t^*),t^*]\frac{w(H,t^*)}{H(t^*)}dt^*\right\} \quad (15a)$$

$$\approx \lambda_t \exp\left[s(z_t)\int_t^{t_p}\frac{w(H,t^*)}{H(t^*)}dt^*\right] \quad (15b)$$

The function of depth $s(z_t)$ is simply a geometric factor describing the time-averaged position of the layer λ_t on the curve $\Upsilon(z,t)$. We calculate this factor from the Raymond-Waddington-Schott model [*Schott et al.*, 1992]. Thus we are neglecting temporal changes in the normalized shape of the strain rate versus depth curve. Instead, we propose maximum plausible changes to $\Upsilon(z,t)$ and use them to define error bars on the inferred accumulation rate. For inferring accumulation rates back to about 35 kyr B.P. the possible variations in $s(z)$ are relatively small, because ice of this age and younger is in the upper two thirds of the ice sheet. Further back in time, there is a marked increase in uncertainty on inferred accumulation rates due to uncertainties in $H(t)$, and due to strong variation of s with increasing depth in the ice sheet (cf. J.F. Bolzan et al., Reconstruction of past accumulation rates from the Greenland Ice Sheet Project 2 ice core data, submitted to *J. Geophys. Res.*, 1996, hereafter referred to as Bolzan et al., submitted manuscript, 1996).

There are two reasons for using the approximate equation (15b) to destrain layers instead of a specific measure of strain resulting from equations (3) and (15a). The first is brevity of computation; equation (15b) only requires us to record $w(H)$ and H through time, rather than calculating and recording integrated strain rates for many layers. The second is the wish to divorce, as well as possible, the temperature computation from the

specific strain predictions of our models. The function w_A insures that vertical heat advection is calculated as accurately as possible for the temperature model, for any given history of accumulation rate or ice sheet geometry. Unfortunately this also renders the solution to (15a) nonunique; inferring accumulation rates requires committing to a strain model. Uncertainties in inferred accumulation rates result from changes in $s(z)$ within the purview of our ice dynamics model, and from deviations of nature from our ice dynamics model. The former we quantify, and they are found to be significantly smaller than the uncertainty due to the unknown marginal retreat distance (see below and Figure 6). The price we pay for the approximation (15b) is therefore small. The latter are essentially unknown until measurements of vertical strain at depth in the GISP2 hole can be made, and may be large.

Results and Discussion

Ice Sheet Thickness and Elevation

All of our calculations show a substantial increase in ice sheet thickness during deglaciation (Figure 2a), in response to the substantial increase of accumulation rate. The thinning as the ice sheet responds to retreat of the margins opposes this, so that if the retreat is large (ΔL = 200 km), there is no net thickness change from the last glacial maximum to the Holocene. In central Greenland, the timescale for thickness changes forced by accumulation rate changes is approximately 2 millennia (Figures 2a and 5; also *Whillans* [1981]), which is similar to the marginal retreat response time, τ_M. But the marginal retreat during deglaciation was less abrupt than the accumulation rate increase. The combination results in a thickness maximum in the early Holocene for marginal retreats greater than approximately 100 km, and a near constant Holocene thickness for ΔL = 100 km.

The corresponding elevation (relative to sea level) histories show a near-constant Holocene elevation for ΔL = 50 km, and a decreasing Holocene elevation for larger retreats (Figure 2b). The calculated Summit elevations during the last glacial maximum vary from 200 m less than at present to 100 m greater than at present. Because the response time of thickness to accumulation rate changes is millennial, the elevations do not mimic the high-frequency fluctuations of the accumulation record, making the elevation a smoother function of time. We do not expect there to have been rapid fluctuations of elevation during the Holocene.

Which of these elevation curves is most reasonable? Geologic evidence indicates the Greenland Ice Sheet margin had extended about 200 km in the southwest part of the island and about 150 km eastward during the last glacial [*Funder*, 1989; *Funder and Larsen*, 1989]. At the latitude of Summit, the western margin position is not well known but was probably at least 100 km extended. Thus we expect the histories

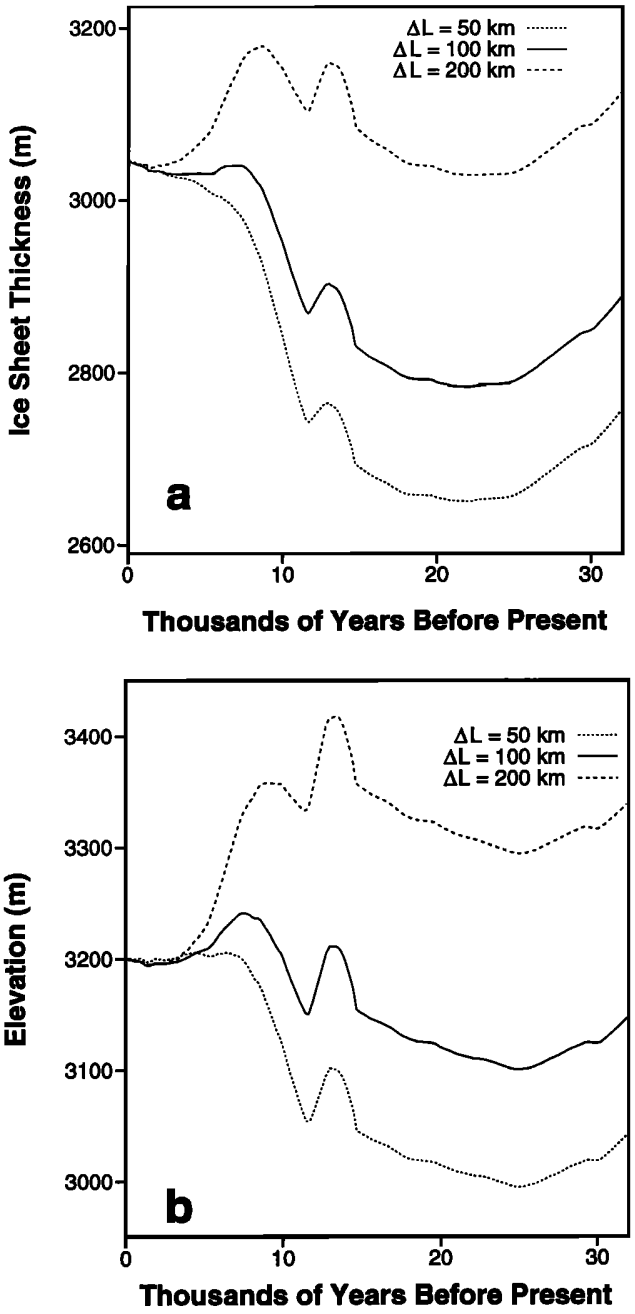

Figure 2. a. Ice sheet thickness through time at GISP2, for three different marginal retreat distances. b. The corresponding elevation histories.

with 100 km < ΔL < 200 km to be most appropriate. However, there are sizable uncertainties due to possible changes in horizontal gradients of accumulation rate, isostatic response and ice rheology, and due to asymmetry of marginal retreat on the east and west. It is thus highly desirable to use an independent elevation proxy to choose which history is most reasonable, if any. Total gas barometry may provide this important information, though total gas data are plagued by high-frequency noise of uncertain origin [*Martinerie et al.*, 1994]. The GISP2 total gas data of Brook and Bender

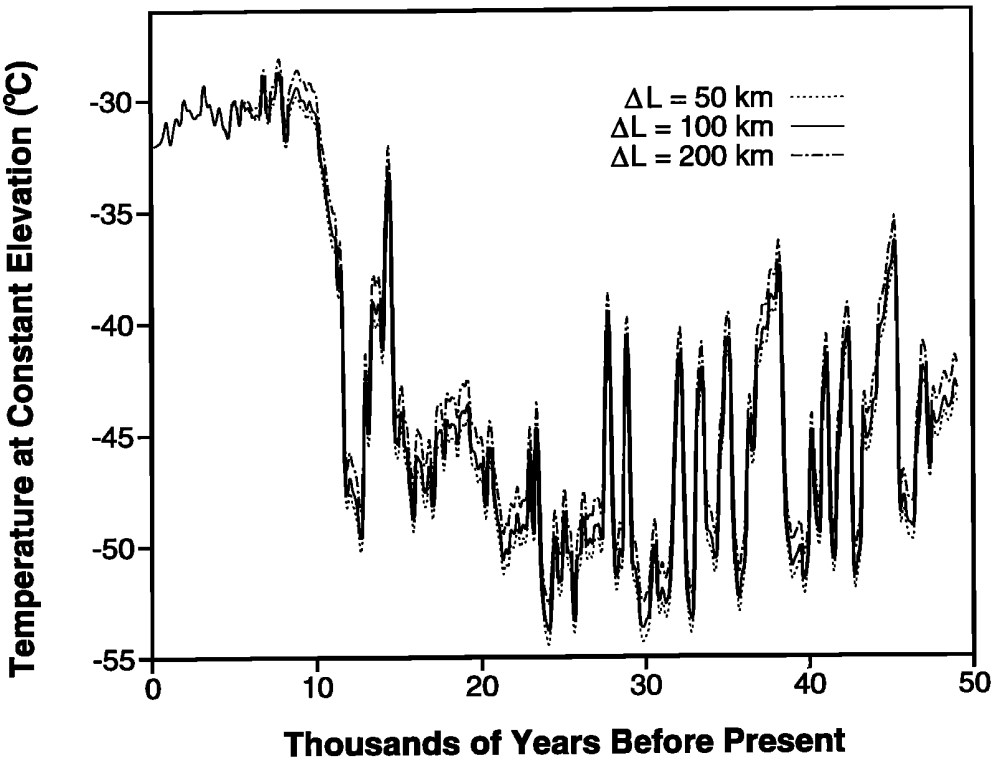

Figure 3. Temperature history according to calibrated isotope curve, corrected for elevation changes. The data have been smoothed with a 250-year triangular filter so that the effect of different elevation corrections, corresponding to different marginal retreat distances, can be seen.

show a moderately higher gas content during the glacial period, after correcting for temperature (E. Brook, pers. comm., 1995). The GRIP data of Raynaud and colleagues likewise show a large decrease in gas content during deglaciation, and in addition show a sizable gas content increase from early to late Holocene [*Raynaud et al.*, this issue]. If elevation changes of the ice sheet are responsible for these trends, then the ice sheet surface must have been at lower elevation during the glacial, have risen during deglaciation, and have decreased elevation again through the Holocene. This pattern compares best with our elevation curves for marginal retreat distances of 100 to 150 km. However, problems with interpretation of total gas content as elevation preclude a firm conclusion at this time.

Temperature

Before examining the temperature results, the reader should appreciate two important points. First, It is unlikely that a single relationship between $\delta^{18}O$ and Greenland surface temperature exists, due to the many factors that affect the isotopic composition of firn in addition to local temperature (these factors are listed and references are cited in *Cuffey et al.* [1995] and *Peel et al.* [1988]). Further, these factors depend on the climate and are likely to vary in importance from one climate state to another. Therefore, rather than choosing a single time-invariant isotope/temperature relationship to calibrate (as do *Johnsen et al.* [1995]), we divide the isotopic history into four periods and allow the calibration to be different in each (see discussion of surface temperature forcing in the Model Components section of this paper).

Second, to facilitate use of our calibration by other researchers, we choose to calibrate the GISP2 $\delta^{18}O$ raw data as given by *Grootes et al.* [1993] and *Stuiver et al.* [1995] without any corrections for changes in sea-water isotopic composition. *This does not noticeably affect the magnitude of the inferred temperature changes.* The magnitude of the inferred temperature changes is determined by the borehole temperature analysis and the shape of the $\delta^{18}O$ history, and is independent of the absolute magnitude of the changes in $\delta^{18}O$. Because sea-water composition and Greenland ice composition are strongly correlated through time, the result of calibrating a sea-water-corrected isotope history is therefore different calibration coefficients in equations (16a) to (16d), not a different temperature history. The only exception at GISP2 is the earliest part of the Holocene (see below), to which the borehole temperatures are not particularly sensitive.

We have found the calibrated $\delta^{18}O$ record to be a good proxy for environmental temperature at Summit [*Cuffey et al.*, 1995], with the following calibration (t in kiloyears before present):

$$T = 3.05\delta^{18}O + 75.4 \qquad t > 8 \qquad (16a)$$

$$T = 3.98\delta^{18}\mathrm{O} + 107.7 \qquad 8 > t > 3 \qquad (16b)$$

$$T = 3.99\delta^{18}\mathrm{O} + 108.0 \qquad 3 > t > 0.5 \qquad (16c)$$

$$T = 2.15\delta^{18}\mathrm{O} + 43.4 \qquad t < 0.5 \qquad (16d)$$

This isotope-based temperature history (Figure 3) is valid at least for the sufficiently long-term average temperature that is resolvable by our borehole temperature analysis [*Cuffey et al.*, 1995]. This averaging length increases back in time from centuries in the late Holocene to a few millennia in the early Holocene to a few tens of millennia at 40ka. Severinghaus and colleagues have subsequently shown that this temperature history is probably also valid on the much shorter timescale of the major climate transitions [*Severinghaus et al.*, 1996]. For ages greater than about 40 ka, the borehole temperature history is largely obscured by poor knowledge of the geothermal heat flux. A more detailed borehole temperature analysis is clearly motivated both by misfit of our best model temperatures to the measurements and by the improved resolution that will accompany analysis of the more recent and accurate temperature measurements of G.D. Clow (manuscript in preparation, 1996). However, these more accurate results should not differ in the inferred long-term averages and should not affect the thickness history. Analysis of the structure of the δ^{18}O history is presented by *Stuiver et al.* [1995] and *Johnsen et al.* [this issue].

We can use the elevation histories to infer a history of temperature at constant elevation (the true climatic change), by assuming a constant lapse rate of 6 °C km^{-1} [*Putnins*, 1970]. The resulting correction to temperature of the last glacial maximum is small compared to the deglacial temperature change; the temperature range is about 1.5 °C for 50 km $\leq \Delta L \leq$ 200 km. More interesting is the correction to the early Holocene temperature record. Here the correction shows a more pronounced early Holocene temperature maximum with a net cooling through the Holocene of 2.5 °to 3 °C, if the large marginal retreat history is applicable (Figure 3). The net cooling through the Holocene is 2 °C for $\Delta L = 50$ km, and in this case the early Holocene is about as warm as the late-mid Holocene.

The δ^{18}O record can be further modified to account for the changing enrichment of seawater due to changes in global ice volume [*Shackleton*, 1987]. Doing so changes the shape of the temperature curve only in the early Holocene, for which the seawater-corrected curve has an increasing isotopic temperature from early to mid Holocene. The resulting calibration provides a slightly worse match to the data than does the noncorrected curve. This, and the higher frequency of melt layers in early Holocene ice [*Alley and Anandakrishnan*, 1995], suggest that possibly the seawater composition correction is inappropriate during deglaciation, perhaps because the isotopic composition of ocean surface waters is not comparable to the bulk composition [*Fisher*, 1992]. We defer this issue until the higher-resolution analyses of Holocene temperature are available.

The large deglacial temperature change indicated by (16a) is a robust result, emerging from both GISP2 and GRIP data, only weakly sensitive to uncertainties in the depth-age scale (*Cuffey et al.*, 1995), and weakly affected by elevation corrections and possible source water composition corrections. Consequently, there seems little doubt that the surface temperature of the ice sheet during the last glacial was some 15 °C colder than present, on average (from 11.5 to 40 ka). However, the question remains to what extent this temperature change applies to the atmosphere above the ice sheet; near-surface temperature inversions often exist above ice sheets, especially in winter, when longwave radiation upward from the ice sheet is not balanced by downward solar radiation or longwave radiation from the atmosphere. The latter depends strongly on the cloudiness of the atmosphere [*Ambach*, 1985]. It is not known how cloudy Summit was during the last glacial, compared to the present, and this precludes a proper calculation of glacial inversion strengths. An heuristic, back-of-the-envelope calculation can be made by recognizing that Summit during the last glacial maximum had a mean annual temperature and accumulation rate similar to modern day South Pole, where the wintertime inversion strength is typically 25 °C [*Warren*, 1996]. Modern winter inversion strengths in central Greenland are approximately 10 °C [*Putnins*, 1970]. These inversions are, on average, negligible in summer, when insolation is high. The mean annual inversion strengths are therefore about half the winter value. The change in mean annual inversion strength from glacial maximum to Holocene at Summit may therefore have been about 6 °C, which is 30% of the net surface temperature change. This is likely an overestimate because Greenland is generally more cloudy than South Pole and has a shorter sunless winter. Thus the atmospheric change was probably also large, but changes in inversion strength were probably not negligible; further investigation is warranted.

Holocene Temperature-Accumulation Relation

The relationship between temperature (T) and accumulation rate ($\dot{b}$) in the Holocene is of fundamental interest because the fate of the Greenland Ice Sheet in a world warmed by anthropogenic greenhouse gases depends on how much increased melting is opposed by increased snowfall [e.g., *Huybrechts et al.*, 1991]. There is a strong positive correlation between accumulation rate and temperature (δ^{18}O) through glacial-interglacial cycles [*Kapsner et al.*, 1995; *Dahl-Jensen et al.*, 1993], which allows the ice sheet to exist stably in the warm climate. *Meese et al.* [1994] apply this correlation to the Holocene; they infer, among other events, an extremely warm period a little over 1 millenium ago, and a recent cooling trend. In contrast, *Kapsner et al.* [1995] argue that accumulation rate and temperature are essentially decoupled in the Holocene (at timescales of years to 1 century) and that changes in the former are due to

Table 1a. The Relationship Between Temperature and Accumulation Rate at Summit for the Past 6500 Years: Residual Moving Average

Half Width of Triangular Filter, kyr	Correlation Coefficient	Sensitivity mm $yr^{-1}\,°C^{-1}$ warming
1.0	-0.79	-6.9
0.4 with 1.0 removed	-0.04	...
0.1 with 0.4 removed	-0.02	...
0.025 with 0.1 removed	0.02	...

The sensitivity is the average change in annual accumulation rate per unit warming. The histories $\dot{b}(t)$ and $T(t)$ are smoothed with triangular average filters of various widths. To isolate high-frequency components of these histories, lower-frequency averages are subtracted from the higher-frequency averages as stated in the table; the result is analogous to a band-passed record. Defining $\bar{b}$ and $\bar{T}$ as the average accumulation rate and temperature for the past 6.5 kyr, the correlation coefficient for the filtered histories $\hat{b}$ and $\hat{T}$ is $r = \left[\int_0^{6.5}(\hat{T}-\bar{T})(\hat{b}-\bar{b})dt\right]\left[\int_0^{6.5}(\hat{T}-\bar{T})^2\,dt\int_0^{6.5}(\hat{b}-\bar{b})^2\,dt\right]^{-1/2}$ and the sensitivity is $\mathrm{sgn}(r)\times\left[\int_0^{6.5}|\hat{b}-\bar{b}|\,dt\right]\left[\int_0^{6.5}|\hat{T}-\bar{T}|\,dt\right]^{-1}$.

changes in the positions of storm tracks, which are not well correlated with temperature changes.

We are now in a better position to evaluate these opposing views, having corrected accumulation rates for ice sheet thickness changes, and having calibrated the isotopic thermometer. The $\dot{b}$ - T relationship is frequency dependent. Most pertinent to anthropogenic climate changes is the relationship averaged over centuries to millennia. Higher frequencies were analyzed by *Kapsner et al.* [1995]. Comparison of the $\dot{b}$ and T histories smoothed to 1-kyr averages shows a strong negative correlation (Tables 1a and 1b; Figure 4), with an average accumulation rate decrease of 0.008 m yr^{-1} per 1 °C warming. Smoothing the records to reveal the half-millennial averages and subtracting out the 1-kyr trend, the remaining, higher-frequency signal still has a negative correlation but a weak one. At 1 to several centuries of smoothing (with the 500-year variation removed) there is essentially no correlation. At less than a century, there is a very weak positive correlation, but the low correlation indicates it is not useful for predictions (Tables 1a and 1b).

Table 1b. The Relationship Between Temperature and Accumulation Rate at Summit for the Past 6500 Years: Band Pass Filtered

Wavelengths Passed kyr	Correlation Coefficient	Sensitivity mm $yr^{-1}\,°C^{-1}$
> 1.0	-0.57	-8.7
0.4 to 1.0	-0.04	...
0.1 to 0.4	0.01	...
< 0.1	0.06	...

The histories $\dot{b}(t)$ and $T(t)$ are smoothed with band pass filters. The sensitivity and correlation coefficient are as defined in Table 1a.

The expected increase of accumulation rate with temperature therefore does not exist at the millennial scale in the Holocene (Figure 4) and is exceedingly weak at the century scale. We concur with *Kapsner et al.* [1995] that accumulation rate is not thermodynamically controlled over centuries in the Holocene but is probably controlled by storm track positions, and we extend this result to the millennial. The most important implication is that the Greenland Ice Sheet is more prone to volume reduction, which contributes to sea level rise, than generally thought [cf. *Kapsner et al.*, 1995]; increased

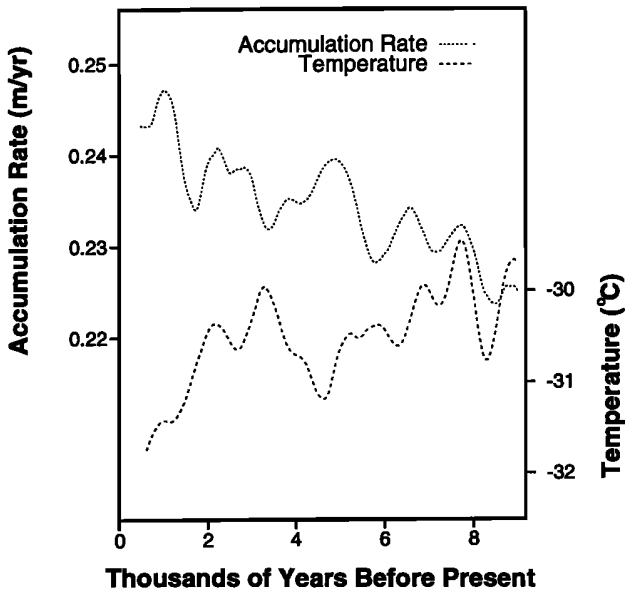

Figure 4. Five-century averages for temperature and accumulation rate for the Holocene (and for ΔL=150 km). Note the switch from correlated to anticorrelated at about 7 kyr B.P. The early Holocene will look different for different ΔL. The mid and late Holocene will not.

melt at the margins of the ice sheet may not be balanced by increased accumulation in the interior. This conclusion could be made stronger if it were shown that the accumulation rate variations at GISP2 accurately reflect accumulation rate variations averaged over a large portion of the ice sheet surface. Another implication is that accumulation rate cannot be used as a thermometer at these timescales. Note that this result is independent of the assumption that $\delta^{18}O$ is a good thermometer, because cooling in the late Holocene is clearly seen in borehole temperatures [*Cuffey et al.*, 1995; *Dahl-Jensen and Johnsen*, 1986; *Cuffey et al.*, 1992], coincident with rising accumulation rates at GISP2.

Glacial Accumulation Rates

The accumulation rate at Summit was substantially less during the last glacial period and changed abruptly at climate transitions [*Alley et al.*, 1993; *Meese et al.*, 1994; *Dahl-Jensen et al.*, 1993]. The abrupt changes are a robust result, because vertical gradients in cumulative strain are small, except possibly very close to the bed or in pure shear regimes where boudinage is possible [*Cunningham and Waddington*, 1990]. However, inferences of the average accumulation rates are sensitive to the dynamic history of the ice sheet, including thickness changes and changes in ice sheet surface curvature. *Cutler et al.* [1995] made a good first attempt at interpreting layer thicknesses while allowing for thickness changes. They found average glacial maximum accumulation rates (from 15 to 30 kyr B.P.) of 6.3 to 7.7 cm yr^{-1}, for marginal retreat distances of 0 to 100 km. We bring two further developments to this pursuit: our thickness history includes the effects of temperature change and approximated nonthermal rheologic changes, and we allow for some nonsteady ice sheet geometry, in the inland response to marginal retreat. These additions result in lower inferred accumulation rates, and reduced sensitivity of the inferred rates

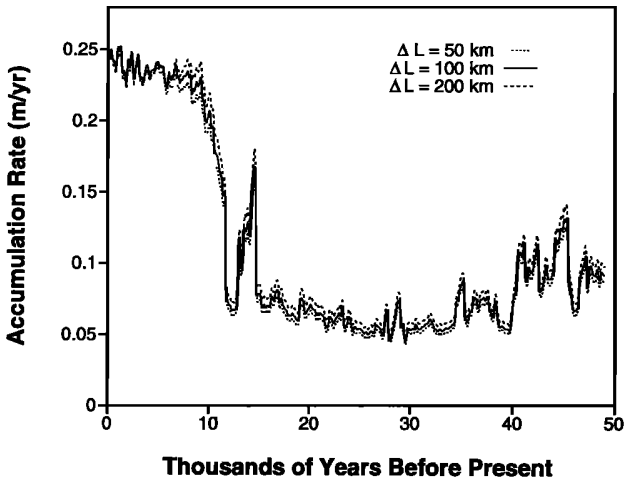

Figure 5. Accumulation rate histories for different marginal retreat distances.

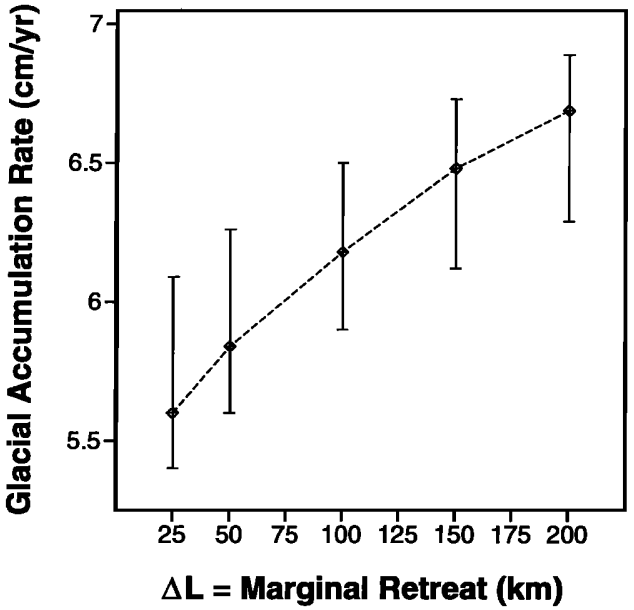

Figure 6. The accumulation rate averaged over the last glacial maximum (15 to 32 kyr B.P.). Error bars correspond to maximum plausible changes in the function $s(z)$. The total uncertainty may be much larger than these.

to the choice of ΔL. We find the average accumulation rate to have been 5.4 to 6.9 cm yr^{-1} for ΔL of 25 to 200 km, respectively (Figures 5 and 6). These agree well with the results of Bolzan et al. (submitted manuscript, 1996) which correspond to small ΔL cases. We suspect that the Cutler et al. calculations over-predict for two reasons. First, they do not include the thinning of the ice sheet due to the penetration of Holocene warmth to the ice sheet bed. Second, they force the extra vertical velocity associated with marginal-retreat-induced thinning to be ascribed to higher accumulation rates, because their ice sheet profile is always a steady state one. Nonetheless, our results are comparable and differ from theirs by less than 1 cm yr^{-1} for small marginal retreats, and by less than 3 cm yr^{-1} for large marginal retreats. Likewise, our results are within 1 to 3 cm yr^{-1} of the original *Alley et al.* [1993] constant-thickness results, for large to small ΔL, respectively, and within 3 cm yr^{-1} of the values implied by equation (2) of *Johnsen et al.* [1995].

A larger uncertainty than the one due to ΔL in this analysis results from poor knowledge of how vertical strain rates vary with depth in nature. Measurement of this deformation at GISP2 will be an important development that will lead to revised accumulation histories.

Conclusion

During the last glacial maximum, central Greenland's climate was severely cold and dry, with average surface temperatures of -50°to -55 °C and accumulation rates of 5.5 to 7 cm yr^{-1}. The sensitivity of Greenland's cli-

mate to changes in forcings (a combination of reduced greenhouse gases, increased surface albedo, increased aerosol loadings, reduced insolation, and possibly others) has been larger than expected. During the mid to late Holocene, accumulation rate and temperature have been essentially uncorrelated at a timescale of a century. Millenial averages of accumulation rate and temperature, however, are clearly negatively correlated. Thus there is no historical basis for expecting increases in accumulation rate to accompany, and oppose, a climatic warming over the ice sheet, though the possibility is not excluded.

Notation

A_o flow law prefactor.
$\bar{A}$ effective ice softness for an ice sheet; a function of A_o, μ, and T.
$a_{1,2,3}$ velocity tuning coefficients.
$\dot{b}$ accumulation rate (thickness of ice per time).
c heat capacity.
f trade-off parameter for weighting function (in J).
g gravitational acceleration.
H ice sheet thickness.
H_d ice sheet thickness at the ice divide.
$\dot{H}_M$ rate of ice divide thinning in response to marginal retreat.
J mismatch index.
j dummy index variable.
k thermal conductivity.
k_r thermal conductivity of bedrock.
L ice sheet half-width.
L_o modern Greenland Ice Sheet half width = 400 km.
ΔL net marginal retreat distance during deglaciation.
N_T temperature change through time at a given depth due to a unit surface temperature perturbation.
n flow law exponent = 3.
Q activation energy for creep of ice.
q_g geothermal heat flux.
R gas constant.
R_T radius of topographic curvature.
r correlation coefficient.
s total strain proportionality function
sgn(x) sign of x.
$\mathcal{S}$ kinematic wave speed.
T temperature.
T_i initial temperature distribution (at 100 kyr B.P.).
$\bar{T}_p$ average temperature of glacial cycles used to calculate T_i.
ΔT_p amplitude of interglacial-glacial temperature cycles used to calculate T_i.
t time (in model, ranges from 100 kyr before present to 0).
t_p model time corresponding to the present.
t_r model time at onset of marginal retreat.
$U(\Delta T_b)$ uniform random temperature describing effects of uncertainties in ancient accumulation rates.
$U(\Delta T_i)$ uniform random temperature describing effects of uncertainties in initial temperature distribution.
$U(\Delta T_\mu)$ uniform random temperature describing effects of uncertainties in ice softness.
$\vec{u}$ horizontal ice velocity.
u_x horizontal ice velocity westward.
u_y horizontal ice velocity northward.
w vertical ice velocity.
w_A vertical ice velocity adjustment function.
w_S vertical ice velocity for steady state geometry.
w_M vertical ice velocity enhancement due to nonsteady geometries.
x horizontal coordinate (west).
y horizontal coordinate (north).
z height above ice sheet bed (negative in bedrock; positive in ice).
z_t height above ice sheet bed of layer deposited at time t.
α change in δ^{18}O per change in temperature.
β δ^{18}O at $T = 0$.
γ effective whole ice sheet diffusivity.
$\hat{\gamma}$ local ice sheet diffusivity.
δ^{18}O ratio of concentrations of ^{18}O to ^{16}O, normalized to that for Standard Mean Ocean Water.
$\dot{\boldsymbol{\epsilon}}$ strain rate tensor.
$\dot{\epsilon}_{zz}$ vertical normal strain rate.
$\Theta(z)$ measured borehole temperatures.
Λ filter describing ice divide thickness response to a unit marginal retreat.
λ_t observed thickness of annual layer deposited at time t.
μ enhancement of ice softness.
ρ density.
$\bar{\rho}$ average density above z.
ρ_i solid ice density = 917 kg m^{-3}.
σ_D weighting function (in J).
σ_t weighting function (in J).
$\boldsymbol{\tau}$ stress tensor.
τ_o plastic yield stress for ice = 1 bar.
τ_a contribution of accessory stresses to second invariant of deviatoric stress tensor.
τ_M response time of ice sheet interior to retreat of the margin.
τ_{xz} dominant shear stress.
Υ proportionality (a function of depth

and time) between $\dot{\epsilon}_{zz}$ and its depth average.

Φ total ice flux per unit width through a vertical plane perpendicular to flow lines.

ω eigenvalues in Λ.

∇_H horizontal gradient operator $= \partial/\partial x + \partial/\partial y$.

$\cdot$ tensor inner product.

$*$ convolution.

$\langle\rangle$ average of quantity enclosed.

Acknowledgments. We are indebted to Ed Waddington for his support of this work and to Pete Lombard, Richard Alley, and Charlie Raymond. David Peel's research on the Antarctic Peninsula had an important role in motivating our own work on temporal calibrations of isotope/temperature relationships. We are also extremely grateful to R. Alley and T. Sowers for access to the GISP2 depth-age scale, and to M. Stuiver for access to the GISP2 oxygen isotope record. Further we thank P. Grootes, T. Braziunas, D. Meese, A. Gow, M. Bender, J. Bolzan, E. Brook, D. Dahl-Jensen, Zachary Gaylord, B. Hallet, S. Johnsen, D. MacAyeal, P. Mayewski, D. Morse, N. Nereson, D. Raynaud, R. Saltus, M. Twickler, and J. White. We also thank SMO, PICO, the 109th ANG, the NSF OPP, NICL, and the USGS. This paper is based, in part, on work supported by a U.S. NSF Graduate Research Fellowship to K.C.

References

Alley, R.B., and S. Anandakrishnan, Variations in melt-layer frequency in the GISP2 ice core: Implications for Holocene summer temperature in central Greenland, *Ann. of Glaciol., 21,* 64-70, 1995.

Alley, R.B., et al., Abrupt increase in Greenland snow accumulation at the end of the Younger Dryas event, *Nature, 362,* 527-529, 1993.

Alley, R.B., and B.R. Koci, Recent warming in central Greenland?, *Ann. of Glaciol., 14,* 6-8, 1990.

Alley, R.B., and I.M. Whillans, Response of the East Antarctica ice sheet to sea-level rise, *J. Geophys. Res., 89*(C4), 6487-6493, 1984.

Ambach, W., Characteristics of the heat balance of the Greenland Ice Sheet for modelling, *J. Glaciol., 31,* 3-12, 1985.

Anandakrishnan, S., R.B. Alley, and E.D. Waddington, Sensitivity of the ice-divide position in Greenland to climate change, *Geophys. Res. Lett., 21,* 441-444, 1994.

Bender, M., T. Sowers, M. Dickson, J. Orchardo, P. Grootes, P. Mayewski, and D. Meese, Climate correlations between Greenland and Antarctica during the past 100,000 years, *Nature, 372,* 663-666, 1994.

Bolzan, J.F., E.D. Waddington, R.B. Alley, and D.A. Meese, Constraints on Holocene ice-thickness changes in central Greenland from the GISP2 ice-core data, *Ann. Glaciol., 21,* 33-39, 1995.

Carslaw, H.S., and J.C. Jaeger *Conduction of Heat in Solids,* 2nd ed., Oxford Univ. Press, New York, 1959.

Cathles, L.M., *The Viscosity of the Earth's Mantle,* Princeton Univ. Press, Princeton, N.J., 1975.

Clow, G.D., R.W. Saltus, and E.D. Waddington, A new high-precision borehole-temperature logging system used at GISP2, Greenland, and Taylor Dome, Antarctica, *J. Glaciol., 42,* 576-584, 1996.

Cuffey, K.M., R.B. Alley, P.M. Grootes, and S. Anandakrishnan, Toward using borehole temperatures to calibrate an isotopic paleothermometer in central Greenland, *Global Planet. Change, 6,* 265-268, 1992.

Cuffey, K.M., R.B. Alley, P.M. Grootes, J.M. Bolzan, and S. Anandakrishnan, Calibration of the δ^{18}O isotopic paleothermometer for central Greenland, using borehole temperatures, *J. Glaciol., 40,* 341-349, 1994.

Cuffey, K.M., G.D. Clow, R.B. Alley, M. Stuiver, E.D. Waddington, and R.W. Saltus, Large Arctic temperature change at the Wisconsin-Holocene glacial transition, *Science, 270,* 455-458, 1995.

Cunningham, J., and E.D. Waddington, Boudinage: A source of stratigraphic disturbance in glacial ice in central Greenland, *J. Glaciol., 36,* 269-272, 1990.

Cutler, N., C.F. Raymond, E.D. Waddington, D.A. Meese, and R.B. Alley, The effect of ice-sheet thickness change on the accumulation history inferred from GISP2 layer thicknesses, *Ann. of Glaciol., 21,* 26-32, 1995.

Dahl-Jensen, D., and S.J. Johnsen, Paleotemperatures still exist in the Greenland Ice Sheet, *Nature, 320,* 250-252, 1986.

Dahl-Jensen, D., S.J. Johnsen, C.U. Hammer, H.B. Clausen, and J. Jouzel, Past accumulation rates derived from observed annual layers in the GRIP ice core from Summit, Central Greenland, in *Ice in the Climate System, NATO ASI Ser. 1,* vol. 12, edited by W.R. Peltier, pp. 517-532, Springer-Verlag, New York, 1993.

Fairbanks, R.G., A 17,000-year glacio-eustatic sea level record: Influence of glacial melting rates on the Younger Dryas event and deep-ocean circulation, *Nature, 342,* 637-642, 1989.

Fisher, D.A., Possible ice-core evidence for a fresh meltwater cap over the Atlantic Ocean in the early Holocene, in *The Last Deglaciation: Absolute and Radiocarbon Chronologies, NATO ASI Ser. 1,* vol. 12, edited by E. Bard and W.S. Broecker, pp. 267-293, Springer-Verlag, New York, 1992.

Funder, S., Quaternary geology of ice-free areas and adjacent shelves of Greenland, in *Quaternary Geology of Canada and Greenland,* vol. 1, edited by R.J. Fulton, chap. 13, pp. 743-769, Geol. Surv. of Can., Ottawa, Ont., 1989.

Funder, S. and H.C. Larsen, Quaternary geology of the shelves adjacent to Greenland, in *Quaternary Geology of Canada and Greenland,* edited by R.J. Fulton, vol. 1, chapter 13, 769-772, Geological Survey of Canada, 1989.

Grootes, P.M., M. Stuiver, J. White, S. Johnsen, and J. Jouzel, Comparison of oxygen isotope records from the GISP2 and GRIP Greenland ice cores, *Nature, 366,* 552-554, 1993.

Huybrechts, P., A. Letreguilly, and N. Reeh, The Greenland Ice Sheet and greenhouse warming, *Global Planet. Change, 89,* 399-412, 1991.

Johnsen, S.J., D. Dahl-Jensen, W. Dansgaard, and N. Gundestrup, Greenland paleotemperatures derived from GRIP bore hole temperature and ice core isotope profiles, *Tellus Ser. B, 47,* 624-629, 1995.

Johnsen, S.J., et al., The δ^{18}O record along the GRIP deep ice core and the problem of possible Eemian climatic instability, *J. Geophys. Res.,* this issue.

Jouzel, J., et al., On the validity of the temperature reconstruction from water isotopes in ice cores, *J. Geophys. Res.,* this issue.

Kapsner, W.R., R.B. Alley, C.A. Shuman, S. Anandakrishnan, and P.M. Grootes, Dominant influence of atmospheric circulation on snow accumulation in Greenland over the past 18,000 years, *Nature, 373,* 52-54, 1995.

Martinerie, P., V.Y. Lipenkov, D. Raynaud, J. Chappellaz, N.I. Barkov, and C. Lorius, Air content paleo record in the Vostok ice core (Antarctica): A mixed record of climatic

and glaciological parameters, *J. Geophys. Res., 99*(D5), 10,565-10,576, 1994.

Meese, D.A., A.J. Gow, P. Grootes, P.A. Mayewski, M. Ram, M. Stuiver, K.C. Taylor, E.D. Waddington, and G.A. Zielinski, The accumulation record from the GISP2 core as an indicator of climate change throughout the Holocene, *Science, 266,* 1680-1682, 1994.

Patankar, S.V., *Numerical Heat Transfer and Fluid Flow,* Hemisphere, Washington D.C., 1980.

Paterson, W.S.B., Why ice-age ice is sometimes "soft", *Cold Reg. Sci. Technol., 20,* 75-98, 1991.

Paterson, W.S.B., *The Physics of Glaciers, 3rd* ed., Pergamon, Tarrytown, N. Y., 1994.

Paterson, W.S.B., and E.D. Waddington, Estimated basal ice temperatures at Crete, Greenland, throughout a glacial cycle, *Cold Reg. Sci. Technol., 12,* 99-102, 1986.

Peel, D.A., R. Mulvaney, and B.M. Davison, Stable-isotope/air-temperature relationships in ice cores from Dolleman Island and the Palmer Land Plateau, Antarctic Peninsula, *Ann. of Glaciol., 10,* 130-136, 1988.

Peltier, W.R., and W.T. Hyde, Glacial isostasy and the ice age cycle, in *The Physical Basis of Ice Sheet Modelling,* edited by E.D. Waddington and J.S. Walder, *IAHS Publ. 170,* 247-260, 1987.

Putnins, P., The climate of Greenland, in *World Survey of Climatology,* vol. 14, *Climates of Polar Regions,* pp. 3-113, Elsevier, New York, 1970.

Raymond, C.F., Deformation in the vicinity of ice divides, *J. Glaciol., 29,* 357-373, 1983.

Raynaud, D., and B. Lebel, Total gas content and surface elevation of polar ice sheets, *Nature, 281,* 289-291, 1979.

Raynaud, D., J. Chappellaz, C. Ritz, and P. Martinerie, Air content along the Greenland Ice Core Project core: A record of surface climatic parameters and elevation in central Greenland, *J. Geophys. Res.,* this issue.

Schott, C., E.D. Waddington, and C.F. Raymond, Predicted time-scales for GISP2 and GRIP boreholes at Summit, Greenland, *J. Glaciol., 38,* 162-168, 1992.

Severinghaus, J.P., E.J. Brook, T. Sowers, and R.B. Alley, Gaseous thermal diffusion as a gas-phase stratigraphic marker of abrupt warmings in ice core climate records, *Eos Trans. AGU, 77*(17), Spring Meet. Suppl., S157, 1996.

Shackleton, N.J., Oxygen isotopes, ice volume and sea level, *Quat. Sci. Rev., 6,* 183-190, 1987.

Shuman, C.A., R.B. Alley, S. Anandakrishnan, J.W.C. White, P.M. Grootes, and C.R. Stearns, Temperature and accumulation at the Greenland summit: Comparison of high-resolution isotope profiles and satellite passive microwave brightness temperature trends, *J. Geophys. Res., 100*(D5), 9165-9177, 1995.

Stuiver, M., P.M. Grootes, and T.F. Braziunas, The GISP2 $\delta^{18}O$ record of the past 16,500 years and the role of the Sun, ocean, and volcanoes, *Quat. Res., 44,* 341-354, 1995.

Vialov, S.S., Regularities of glacial shields movement and the theory of plastic viscous flow, *IAHS Publ., 47,* 266-275, 1958.

Warren, S.G., *Antarctica,* in *Encyclopedia of Climate and Weather,* pp. 32-39, New York, Oxford University Press, 1996.

Whillans, I.M., Reaction of the accumulation zone portions of glaciers to climatic change, *J. Geophys. Res., 86*(C5), 4274-4282, 1981.

Whillans, I.M. and W.A. Cassidy, Catch a falling star: Meteorites and old ice, *Science, 222,* 55-57, 1983.

Yen, Y.-C. Review of thermal properties of snow, ice and sea ice, *CRREL Rep. 81-10,* Cold. Reg. Res. and Eng. Lab., Hanover, N.H., 1981.

G. D. Clow, U. S. Geological Survey, Climate History Program, MS-980, Denver, CO 80225. (email: clow@usgs.gov)

K. M. Cuffey, Department of Geological Sciences, Box 351310, University of Washington, Seattle, WA 98195. (email: cuff@geophys.washington.edu)

(Received December 4, 1995; revised July 22, 1996; accepted December 1, 1996.)